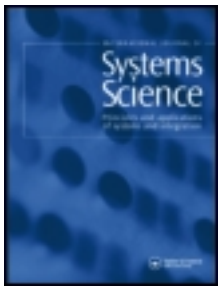

International Journal of Systems Science
Publication details, including instructions for authors and subscription information:
http://www.tandfonline.com/loi/tsys20

Mobile-robot pose estimation and environment mapping using an extended Kalman filter

Gregor Klančar [a], Luka Teslić [a] & Igor Škrjanc [a]
[a] Faculty of Electrical Engineering, University of Ljubljana, Ljubljana, Slovenia
Version of record first published: 05 Mar 2013.

To cite this article: Gregor Klančar , Luka Teslić & Igor Škrjanc (2013): Mobile-robot pose estimation and environment mapping using an extended Kalman filter, International Journal of Systems Science, DOI:10.1080/00207721.2013.775379

To link to this article: http://dx.doi.org/10.1080/00207721.2013.775379

International Journal of Systems Science, 2013
http://dx.doi.org/10.1080/00207721.2013.775379

RESEARCH ARTICLE

Mobile-robot pose estimation and environment mapping using an extended Kalman filter

Gregor Klančar*, Luka Teslić and Igor Škrjanc

Faculty of Electrical Engineering, University of Ljubljana, Ljubljana, Slovenia

(*Received 4 April 2011; final version received 28 September 2012*)

In this paper an extended Kalman filter (EKF) is used in the simultaneous localisation and mapping (SLAM) of a four-wheeled mobile robot in an indoor environment. The robot's pose and environment map are estimated from incremental encoders and from laser-range-finder (LRF) sensor readings. The map of the environment consists of line segments, which are estimated from the LRF's scans. A good state convergence of the EKF is obtained using the proposed methods for the input- and output-noise covariance matrices' estimation. The output-noise covariance matrix, consisting of the observed-line-features' covariances, is estimated from the LRF's measurements using the least-squares method. The experimental results from the localisation and SLAM experiments in the indoor environment show the applicability of the proposed approach. The main paper contribution is the improvement of the SLAM algorithm convergence due to the noise covariance matrices' estimation.

Keywords: wheeled mobile robot; localisation; mapping; extended Kalman filter

1. Introduction

Simultaneous localisation and mapping (SLAM) is one of the key problems to be solved for autonomous mobile-robot operation in an unknown environment. A robot with no prior environment information needs to build a consistent map of the environment by moving through the environment and then use this map to localise, plan and control its motion at the same time.

1.1. The problem description

In SLAM a state vector consists of the robot's pose and the observed locations of the environment features. In an extended Kalman filter (EKF) all the state variables are correlated through the covariance matrix, which means that the observation of each feature affects the estimate of other features in the map. Therefore, every observation requires that the complete state vector, as well as the covariance matrix, is updated. As a consequence, the computational complexity of the EKF grows quadratically with the number of estimated states (Durrant-Whyte and Bailey 2006).

In EKF based and other SLAM approaches usually only an ad hoc tuning of stochastic modelling parameters is made (uncertainties defined by covariance matrices) to deal with model approximations on the predicted pose (Borges and Aldon 2003). However, appropriate adjustments of these modelling parameters are required to achieve a good performance of EKF estimators such as stability and convergence. Also a feature matching process can be done more efficiently if an appropriate weighting using these modelling parameters is used in the Mahalanobis distance. If input or output uncertainties propagate through nonlinear relation to the filter states or observations the appropriate covariances can be estimated using linearisation of these nonlinearities. Good estimation results in case of nonlinearities can also be obtained using unscented transform (UT) (Hartikainen, Solin, and Särkkä 2011).

In this paper, we propose a novel technique for on-line estimation of stochastic modelling parameters which contribute to a better performance regarding EKF convergence and stability and to a more reliable feature matching process. The input-noise covariance matrix of the EKF is derived from the known noise variances of the angular-velocity measurements of both robot wheels, while the covariance matrix of the line-equation parameters (the output-noise covariance matrix) is estimated from the laser-range-finder's (LRF) scan by the proposed least-squares (LSQ) method applying the linearisation of noise propagation. For the proposed method of observation uncertainty estimation some directions, validation and comparison to unscented transform (UT) are presented. We aim to obtain computational efficient methods for estimation of noise covariance matrices. The analysis of how the estimated robot pose uncertainty is affected according to the proposed line segment parameters uncertainty estimation is also performed. The contribution of this work is also an extension of localisation approach described in our previous work (Teslić, Škrjanc, and Klančar 2010a) to the SLAM approach with a detailed description and experimental evaluation. Evaluations of the proposed algorithms are provided

*Corresponding author. Email: gregor.klancar@fe.uni-lj.si

by experiments on a Pioneer 3-AT mobile robot and also by a comparison to the Monte-Carlo based SLAM software Mapper3 from MobileRobots Inc. (MobileRobots 2009) which has been used and verified by many researchers. The disadvantage of our method is that it requires line features to be estimated from the environment which can be less reliable in unstructured environments. The proposed SLAM approach can be applied to other mobile systems and it can also be upgraded with obstacle avoidance and path planning capabilities as in Pozna, Troester, Precup, Tar, and Preitl (2009) and Dakulović and Petrović (2011) to achieve fully autonomous SLAM mission.

1.2. Prior work

In Thrun (2002) a comprehensive survey of the SLAM problem in mobile robotics is presented, and in literature, many approaches and algorithms involved in solving the SLAM, localisation and mapping problem have been proposed.

Many approaches (Bailey and Durrant-Whyte 2006) have been developed to reduce computational complexity and the associated computation by usually implementing conservative and less accurate algorithms such as information matrix for SLAM, partitioned updates of local map regions, submapping methods and the like. A topological map and a metric map are combined in Tomatis, Nourbakhsh, and Siegwart (2003) and switched state-space models for robot localisation were introduced in Baltzakis and Trahanias (2003). In Bošnak, Matko, and Blažič (2012) a lover complexity of the Kalman filter localisation is achieved by supposing constant covariances and time invariant process which result in constant Kalman gains. A computational efficient localisation using principal component analysis on laser range data is provided in Crowley, Wallner, and Schiele (1998), while Diosi and Kleeman (2007) suggest a laser scan matching approach in polar coordinates. A non-parametric representation of the environment using maximum-likelihood subsets of the data points obtained by LRF is suggested in Delius and Burgard (2010). A real-time mapping obtained by LRF's data histograms correlation is proposed in Rofer (2002), Petri net-based localisation of a mobile robot is developed in Lee and Chung (2006) and visual localisation approach using features extracted from environment is presented in Xu, Han, Tan, and Li (2009) and Wu and Qin (2011). In the presented paper the focus is given to the computational efficient methods for an accurate estimation of covariances which contribute to the SLAM convergence and stability.

Environment representation is often obtained by line segments as in Veeck and Veeck (2004) and Latecki, Sobel, and Lakaemper (2009). A fuzzy approach to line segments extraction algorithm is introduced in Borges and Aldon (2004) and a robust iterative regression model for line segments extraction with outliers detection is presented in Zhang, Rad, and Wong (2008). Borges and Aldon (2003) propose a robust Kalman-filter-based pose estimation using weighted least-square algorithm for outliers rejection. In Nguyen, Gächter, Martinelli, Tomatis, and Siegwart (2007) a comparison of line-extraction algorithms using a 2D LRF is reported. Based on this comparison a split-and-merge algorithm is chosen in this paper because of its good speed and correctness. The EKF-based localisation algorithm for structured environments is shown in Teslić et al. (2010a). Accurate and computationally efficient least-squares approach for line parameters and their covariances estimation from LRF scan is used in this work.

One of the challenges is also an appropriate selection of stochastic parameters which affect the overall SLAM operation (Borges and Aldon 2003). For nonlinear systems an Unscented Kalman Filter (UKF) is proposed where unscented transformation (UT) is used to estimate uncertainties (Hartikainen et al. 2011). In Sakai and Kuroda (2010) a learning technique to help developers to adjust the UKF parameters (input- and measurement-noise covariance matrices and unscented transformation parameters) for an accurate localisation is used. In this work a statistical analysis of a lineralisation approach and UT is made to estimate covariances of the line segment nonlinear transformation. It is established that UT method does not bring any noticeable advantage over the proposed method using linearisation which means that nonlinearity of noise propagation function can be approximated by a less computationally expensive linearisation approach. UT method may become beneficial only if the noise level of the applied LRF (Sick LMS200) would be much higher than currently estimated in the experiments.

This paper is organised as follows. In Section 2 there is a description of the wheeled mobile robot and the environment represented by the extracted line features. Here, the robot kinematics and noise models described by the covariance matrices of the input noise and the line parameters are estimated. Section 3 defines the prediction and correction steps of the SLAM algorithm using the EKF approach. In Section 4 the results of the SLAM algorithm implemented on the Pioneer 3-AT robot in an indoor, structured environment are presented. The paper is concluded in Section 5.

2. Mobile robot and the environment

The Pioneer 3-AT four-wheel mobile robot (Figure 1) was used in an indoor environment that can be described by line segments. The mobile robot has no prior information about the environment where it operates, and therefore it has to construct the map of its environment and simultaneously use this map for localisation. The SLAM algorithm uses only information from incremental encoder sensors attached to the wheels and the LRF Sick LMS200 (Figure 1).

Figure 1. Wheeled Pioneer 3-AT mobile robot with laser range scanner Sick LMS200.

The robot's kinematic model, required to predict the robot's pose, is given by

$$\mathbf{x}_p(k+1) = \mathbf{f}(\mathbf{x}_p(k), \mathbf{u}(k))$$
$$\mathbf{x}_p(k+1) = \begin{bmatrix} x_r(k) + \frac{TR}{2}(\omega_R(k) + \omega_L(k))\cos(\varphi_r(k)) \\ y_r(k) + \frac{TR}{2}(\omega_R(k) + \omega_L(k))\sin(\varphi_r(k)) \\ \varphi_r(k) + \frac{TR}{L}(\omega_R(k) - \omega_L(k)) \end{bmatrix}, \quad (1)$$

where $\mathbf{x}_p(k) = [x_r(k),\ y_r(k),\ \varphi_r(k)]^T$ is the robot's pose at the time instant k, T is the sampling time, R is robot wheel's radius, L is the intermediate wheel distance and $\mathbf{u} = [\omega_R,\ \omega_L]$ are incremental encoder measurements of the right and left wheels' rotational speed, respectively. $\mathbf{u}$ is subject to an error due to the approximate odometry model (1), the measurement noise, the sliding of the wheels (when $\omega_R(k) \neq \omega_L(k)$), as follows

$$\mathbf{u}(k) = \mathbf{u}_n(k) + \mathbf{v}(k), \quad (2)$$

where $\mathbf{u}_n(k)$ is a vector of the nominal wheel speeds and $\mathbf{v}(k)$ is the measurement error. The nature of the measurement error $\mathbf{v}(k)$ is modelled as the zero mean Gaussian noise with the standard deviations being proportional to the rotational speed ($\sigma_L = \delta|\omega_L|$, $\sigma_R = \delta|\omega_R|$). The covariance matrix of $\mathbf{v}(k)$ is the input-noise covariance matrix $\mathbf{Q}(k)$ defined as

$$\mathbf{Q}(k) = \begin{bmatrix} \delta^2\omega_R^2(k) + \alpha^2 & 0 \\ 0 & \delta^2\omega_L^2(k) + \alpha^2 \end{bmatrix}, \quad (3)$$

where δ and α are positive constants estimated conservatively by experiments so that the estimated input uncertainty is higher or equal to the true input uncertainty ($\delta = 0.1$ and $\alpha = 0.001$). The constant α increases EKF stability in case of no motion ($\omega_R = \omega_L = 0$).

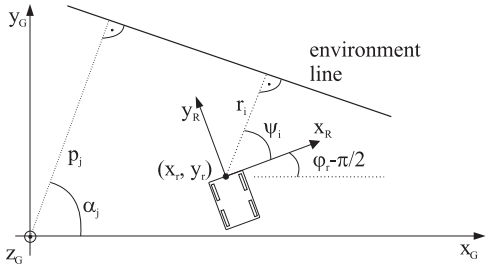

Figure 2. The line parameters (p_i, α_i) according to the global coordinates, and the line parameters (r_i, ψ_i) according to the robot coordinates.

During each time step the robot observes the environment by extracting the line parameters from the observed LRF's reflection points. The scanning range of the LRF Sick LMS200 is 180° with a 1° resolution, which gives the laser-beam angles $\theta_s = [0^\circ, ..., 180^\circ]$ with an associated set of distances $\mathbf{d}_s = [d_{s0^\circ}, ..., d_{s180^\circ}]$ to the obstacles (e.g., a wall). From the reflection points the line segments are identified by the edge points and the normal line parameters ψ_i and r_i expressed in the local robot frame (Figure 2)

$$x_R \cos\psi_i + y_R \sin\psi_i = r_i. \quad (4)$$

The line parameters in each LRF scan are estimated as follows:

- Consecutive reflection points

$$\mathbf{x}_{\text{scan}}(m) = \mathbf{d}_s(m)\cos\theta_s(m)$$

$$\mathbf{y}_{\text{scan}}(m) = \mathbf{d}_s(m)\sin\theta_s(m)$$

  are calculated for all the laser beams where $m = 1, \ldots, 180$.
- The points where the reflections occurred with $\mathbf{d}_s(m) < R_{\text{LRF}}$ (R_{LRF} is LRF's distance range) form an initial cluster. This cluster is then split into more clusters if the distance between consecutive points exceeds the expected smallest threshold distance T_S (e.g., $T_S = 0.15$ m).
- Clusters having at least $N_{\min}$ points (e.g., $N_{\min} = 5$) are retained because they provide a reliable representation of the environment line segments. Having $N_{\min} > 2$ improves the line parameters' estimation because the LRF's noise is averaged.
- To obtain the final consecutive clusters belonging to the environment line segments the split-and-merge algorithm (Nguyen et al. 2007) is applied. Clusters of points that cannot represent a single line segment are split. The process repeats until all the points in each of the clusters can reliably fit the line segment

(their distance from the line is below a predefined threshold). The split-and-merge algorithm is, compared to other line-extraction parameters such as the Hough transform (Schiele and Crowley 1994; Larsson, Forsberg, and Wernersson 1996; Giesler, Graf, Dillmann, and Weiman 1998; Pfister, Roumeliotis, and Burdick 2003), computationally more effective, gives good results and also provides the edge points of the line segments, which is important information for localisation and map building.

- The least-squares method (LSQ) is used for line fitting inside the identified clusters. Each cluster of points $(\mathbf{x}, \mathbf{y})$ is then reduced to the parameters r and ψ of the line equation in normal form according to the robot's coordinates. As shown in our previous work (Teslić, Škrjanc, and Klančar 2010b) the classical LSQ can be efficiently used to estimate the parameters of an explicit line equation

$$y_R = k_l \cdot x_R + c_l.$$

To have a well-conditioned estimation problem the set of points $(\mathbf{x}, \mathbf{y})$ with an estimated line slope $|k_l|$ greater than one is first rotated by $-\frac{\pi}{2}$ by simply exchanging the vector $\mathbf{x}$ with the vector $\mathbf{y}$ and the vector $\mathbf{y}$ with the vector $-\mathbf{x}$. The set of line-segment points $(\mathbf{x}, \mathbf{y})$ is then reduced to the parameters r and ψ of the line equation in normal form (4), as follows

$$\begin{aligned} \mathbf{y} &= [\mathbf{y}(1), \ldots, \mathbf{y}(n)]^T \\ \mathbf{U} &= \begin{bmatrix} \mathbf{x}(1) & \cdots & \mathbf{x}(n) \\ 1 & \cdots & 1 \end{bmatrix}^T \\ \hat{\theta} &= [\hat{k}_l, \hat{c}_l]^T = (\mathbf{U}^T\mathbf{U})^{-1}\mathbf{U}^T\mathbf{y}, \end{aligned} \tag{5}$$

$$r(\hat{k}_l, \hat{c}_l) = \frac{\hat{c}_l}{\sqrt{\hat{k}_l^2 + 1}} \operatorname{sign}(\hat{c}_l),$$

$$\psi(\hat{k}_l) = \arctan 2 \left(\frac{\operatorname{sign}(\hat{c}_l)}{\sqrt{\hat{k}_l^2 + 1}}, \frac{-\hat{k}_l}{\sqrt{\hat{k}_l^2 + 1}} \operatorname{sign}(\hat{c}_l) \right) \tag{6}$$

where n denotes the number of points that correspond to the line segment and the function $\arctan 2$ is a four-quadrant arctan function.

To perform the correction step of the EKF, the covariance matrix $\mathbf{R}_i$ of the estimated line parameters vector of the ith line segment $[r_i, \psi_i]$ also needs to be estimated. Firstly, the covariance matrix of the line parameters $[\hat{k}_l,\ \hat{c}_l]$ is estimated from Equation (5)

$$\mathbf{Z} = \begin{bmatrix} \operatorname{var}(\hat{\mathrm{k}}_\mathrm{l}) & \operatorname{cov}(\hat{k}_l, \hat{c}_l) \\ \operatorname{cov}(\hat{c}_l, \hat{k}_l) & \operatorname{var}(\hat{c}_l) \end{bmatrix} = \operatorname{var}(\mathbf{y}(j))(\mathbf{U}^T\mathbf{U})^{-1}, \tag{7}$$

where

$$\operatorname{var}(\mathbf{y}(j)) = \frac{\sum_{j=1}^{n} (\mathbf{y}(j) - \hat{\mathbf{y}}(j))^2}{n-1}, \ \hat{\mathbf{y}}(j) = \hat{k}_l \cdot \mathbf{x}(j) + \hat{c}_l$$

and $\operatorname{var}(\mathbf{y}(j))$ is the vertical-error variance of the line-segment points $(\mathbf{x}(j),\ \mathbf{y}(j))$ $(j = 1, \ldots, n)$ according to the estimated line with the parameters $\hat{k}_l$ and $\hat{c}_l$ (7). Considering the relation between the explicit (7) and the normal line parameters (8) the covariance matrix $\mathbf{R}_i$ is given by

$$\mathbf{R}_i = \begin{bmatrix} \operatorname{var}(\mathrm{r_i}) & \operatorname{cov}(r_i, \psi_i) \\ \operatorname{cov}(\psi_i, r_i) & \operatorname{var}(\psi_i) \end{bmatrix}, \tag{8}$$

where

$$\begin{aligned} \operatorname{var}(\psi) &= K_{\psi k}^2 \operatorname{var}(\hat{k}_l) \\ \operatorname{var}(r) &= K_{rk}^2 \operatorname{var}(\hat{k}_l) + K_{rc}^2 \operatorname{var}(\hat{c}_l) \\ &\quad + 2K_{rk}K_{rc} \cdot \operatorname{cov}(\hat{k}_l, \hat{c}_l) \\ \operatorname{cov}(r, \psi) &= K_{rk}K_{\psi k} \operatorname{var}(\hat{k}_l) + K_{rc}K_{\psi k} \cdot \operatorname{cov}(\hat{k}_l, \hat{c}_l) \\ \operatorname{cov}(\psi, r) &= \operatorname{cov}(r, \psi) \end{aligned} \tag{9}$$

and

$$\begin{aligned} K_{rk} &= \frac{-\hat{c}_l\hat{k}_l}{\sqrt{\hat{k}_l^2 + 1}(\hat{k}_l^2 + 1)} \operatorname{sign}(\hat{c}_l), \\ K_{rc} &= \frac{\operatorname{sign}(\hat{c}_l)}{\sqrt{\hat{k}_l^2 + 1}}, \quad K_{\psi k} = \frac{\operatorname{sign}(\hat{c}_l)}{\hat{k}_l^2 + 1}, \end{aligned} \tag{10}$$

where gains in Equation (10) are obtained using the linearisation of Equation (6) around the current values of explicit line parameters. A detailed analysis of observation covariance estimation $\mathbf{R}_i$ and its comparisons to alternative approaches are given in Subsection 3.3.

3. SLAM using extended Kalman filter

The EKF approach, which consists of a prediction and a correction step, is adopted here for the purpose of SLAM.

3.1. *Prediction step*

Let $\hat{\mathbf{x}}(k|k) = [\hat{\mathbf{x}}_p(k|k)^T\ ,\ \hat{\mathbf{x}}_m(k|k)^T]^T$ denote a state estimate (at time k) consisting of the estimated robot pose $\hat{\mathbf{x}}_p(k|k)$ and the estimated line-feature parameters in a global map $\hat{\mathbf{x}}_m(k|k) = [\hat{\mathbf{l}}_1, \ldots, \hat{\mathbf{l}}_n]^T$, where $\hat{\mathbf{l}}_i = [p_i\ ,\ \alpha_i]^T$, $i = 1, \ldots, n$ are already mapped line-feature parameters expressed in a global (map) coordinate frame (Figure 2) as follows:

$$x_G \cos\alpha_i + y_G \sin\alpha_i = p_i.$$

The covariance matrix of the state-estimation error at time k is denoted as $\mathbf{P}(k|k)$. In the prediction step the state estimate $\hat{\mathbf{x}}(k|k-1)$ and the state-estimation covariance matrix $\mathbf{P}(k|k-1)$ are predicted based on previous estimates $\hat{\mathbf{x}}(k-1|k-1)$, $\mathbf{P}(k-1|k-1)$ and the odometry model (1). The covariance matrix $\mathbf{P}(k|k-1)$ is structured of the blocks belonging to the robot pose $\mathbf{P}_{pp}$, the blocks belonging to the map features $\mathbf{P}_{mm}$ and the blocks due to correlations between the robot pose and the map features $\mathbf{P}_{pm}$.

$$\mathbf{P}(k|k-1) = \begin{bmatrix} \mathbf{P}(k|k-1)_{pp} & \mathbf{P}(k|k-1)_{pm} \\ \mathbf{P}(k|k-1)_{pm}^T & \mathbf{P}(k|k-1)_{mm} \end{bmatrix}.$$

The prediction step of the EKF is then defined as follows:

$$\begin{aligned} \hat{\mathbf{x}}_p(k|k-1) &= \mathbf{f}(\hat{\mathbf{x}}_p(k-1|k-1), \mathbf{u}(k)) \\ \hat{\mathbf{x}}_m(k|k-1) &= \hat{\mathbf{x}}_m(k-1|k-1) \\ \mathbf{P}(k|k-1)_{pp} &= \mathbf{F_x}\mathbf{P}(k-1|k-1)_{pp}\mathbf{F_x}^T + \mathbf{F_u}\mathbf{Q}(k)\mathbf{F_u}^T \\ \mathbf{P}(k|k-1)_{pm} &= \mathbf{F_x}\mathbf{P}(k-1|k-1)_{pm} \\ \mathbf{P}(k|k-1)_{mm} &= \mathbf{P}(k-1|k-1)_{mm}, \end{aligned} \tag{11}$$

where $\mathbf{F_x} = \frac{\partial \mathbf{f}}{\partial \mathbf{x}_p} |_{(\hat{\mathbf{x}}_p(k-1|k-1), \mathbf{u}(k))}$ is the jacobian of Equation (1) with respect to $\mathbf{x}_p$, $\mathbf{F_u} = \frac{\partial \mathbf{f}}{\partial \mathbf{u}} |_{(\hat{\mathbf{x}}_p(k-1|k-1), \mathbf{u}(k))}$ is the jacobian of Equation (1) with respect to noise in the input $\mathbf{u}$ and $\mathbf{Q}(k)$ is defined in Equation (3).

3.2. *Correction step*

The correction step of the EKF is performed when new observations of the line parameters (see Equation (4)) $\mathbf{z}(k)$ are available.

3.2.1. *Line association problem*

For each observation $[r_j, \psi_j]^T$ in $\mathbf{z}(k)$ a possible feature pair in a state vector $\hat{\mathbf{x}}_m(k|k-1)$ (global map) with index $i = 1, \ldots, n$ must be found. The matching strategy for determining whether the observed feature is already present in the global map (state vector $\hat{\mathbf{x}}_m(k|k-1)$) is adopted from Garulli, Giannitrapani, Rossi, and Vicino (2005). Some other matching approaches can also be found in Pfister et al. (2003) and Anousaki and Kyriakopoulos (2007).

The observation is transformed to global coordinates (see Equation (13)) as follows:

$$\begin{aligned} Di &= r_j - \hat{x}_r(k|k-1)\sin(\psi_j + \hat{\varphi}_r(k|k-1)) \\ &\quad + \hat{y}_r(k|k-1)\cos(\psi_j + \hat{\varphi}_r(k|k-1)) \\ \begin{bmatrix} \hat{p}_j \\ \hat{\alpha}_j \end{bmatrix} &= \mathbf{g}(\hat{\mathbf{x}}_p\left(k|k-1\right), r_j, \psi_j\right) \\ &= \begin{bmatrix} |Di| \\ \psi_j + (\hat{\varphi}_r(k|k) - \frac{\pi}{2}) - (-0.5 \times \mathrm{sign}(Di) + 0.5)\pi \end{bmatrix}. \end{aligned}$$

A covariance matrix for the observed line parameters $[\hat{p}_j, \hat{\alpha}_j]^T$ is determined as follows:

$$\mathbf{S} = \mathbf{G_x}\mathbf{P}(k|k-1)\mathbf{G_x}^T + \mathbf{G_z}\mathbf{R_j}\mathbf{G_z}^T,$$

where

$$\begin{aligned} \mathbf{G_x} &= \frac{\partial \mathbf{g}}{\partial \hat{\mathbf{x}}_p}\bigg|_{(\hat{\mathbf{x}}_p(k|k-1), r_j, \psi_j)} \\ &= \begin{bmatrix} -d_i \sin(\psi_j + \hat{\varphi}_r(k|k-1)) & 0 \\ d_i \cos(\psi_j + \hat{\varphi}_r(k|k-1)) & 0 \\ o_i & 1 \end{bmatrix}^T \\ \mathbf{G_z} &= \frac{\partial \mathbf{g}}{\partial [r_j, \psi_j]^T}\bigg|_{(\hat{\mathbf{x}}_p(k|k-1), r_j, \psi_j)} = \begin{bmatrix} d_i & o_i \\ 0 & 1 \end{bmatrix}, \end{aligned}$$

where $d_i = \mathrm{sign}(Di)$, $o_i = -d_i\hat{x}_r(k|k-1)\cos(\psi_j + \hat{\varphi}_r(k|k-1)) - d_i\hat{y}_r(k|k-1)sin(\psi_j + \hat{\varphi}_r(k|k-1))$ and $\mathbf{R}_j$ is the observation covariance matrix defined in Equation (10). The observed line segment $[\hat{p}_j, \hat{\alpha}_j]^T$ is compared to all line segments $[p_i, \alpha_i]^T$, $i = 1, \ldots, n$ whose end points are in the neighbouring region defined by the current pose estimate and LRF range R_{LRF}. A possible pair minimises the weighted distance

$$d_m = \left(\begin{bmatrix} p_i \\ \alpha_i \end{bmatrix} - \begin{bmatrix} \hat{p}_j \\ \hat{\alpha}_j \end{bmatrix}\right)^T \mathbf{S}^{-1} \left(\begin{bmatrix} p_i \\ \alpha_i \end{bmatrix} - \begin{bmatrix} \hat{p}_j \\ \hat{\alpha}_j \end{bmatrix}\right) \tag{12}$$

and fulfils the condition $d_m < T_m$, where T_m is the threshold value (e.g., $T_m = 0.5$). To find a valid line-feature pair the edge points of the observed line segment and the mapped feature are also compared to check whether the observed line segment lies on the mapped line segment. The edge points of the mapped features are not included in the state vector. They are only used for the matching process and are updated with the correction step of the EKF. The observations with no pair are considered as newly observed features.

The observation of line parameters is denoted as $\mathbf{z}(k) = [\mathbf{z}_M(k)^T, \mathbf{z}_N(k)^T]^T$, where $\mathbf{z}_M(k) = [r_1, \psi_1, \ldots, r_M, \psi_M]^T$ are features of already observed line segments that are present in the global map and $\mathbf{z}_N(k) = [r_{M+1}, \psi_{M+1}, \ldots, r_{M+N}, \psi_{M+N}]^T$ are newly observed features that are not present in the global map. The observed line features $\mathbf{z}_M(k)$ are used to update the state estimate $\hat{\mathbf{x}}(k|k)$, while the newly observed features $\mathbf{z}_N(k)$ are appended to $\hat{\mathbf{x}}(k|k)$.

For each observation in $\mathbf{z}_M(k)$ with index $j = 1, \ldots, M$ a match exists in the global map $\hat{\mathbf{x}}_m(k|k-1)$ with the index $i \in 1, \ldots, n$, where M is the number of observations in $\mathbf{z}_M(k)$ and n is the number of all the mapped features in $\hat{\mathbf{x}}_m(k|k-1)$. The parameters p_i and α_i of the matching line segment from the global map (according to the global coordinates) are transformed into the parameters $\hat{r}_j$ and $\hat{\psi}_j$

(according to the coordinates of the robot) by

$$Ci = p_i - \hat{x}_r(k|k-1)\cos(\alpha_i) - \hat{y}_r(k|k-1)\sin(\alpha_i),$$
$$\begin{bmatrix} \hat{r}_j \\ \hat{\psi}_j \end{bmatrix} = \mathbf{h}_j(\hat{\mathbf{x}}_p(k|k-1), p_i, \alpha_i) =$$
$$\begin{bmatrix} |Ci| \\ \alpha_i - \left(\hat{\varphi}_r(k|k-1) - \frac{\pi}{2}\right) + \frac{1}{2}(-\text{sign}(Ci) + 1)\pi \end{bmatrix}, \quad (13)$$

where $\mathbf{h}_j(\cdot)$ is the observation model and $\hat{\mathbf{x}}_p(k|k-1)$ (11) is the prediction of the robot's pose.

3.2.2. Correction step for already observed features

The predicted observations $\hat{\mathbf{z}}_M(k|k-1)$ for the already observed features $\mathbf{z}_M(k)$ are, according to Equation (13), given by

$$\hat{\mathbf{z}}_M(k|k-1) = \begin{bmatrix} \mathbf{h}_1(\hat{\mathbf{x}}_p(k|k-1), p_1, \alpha_1) \\ \vdots \\ \mathbf{h}_M(\hat{\mathbf{x}}_p(k|k-1), p_M, \alpha_M) \end{bmatrix}. \quad (14)$$

The observation jacobian of Equation (13) for the jth observation is $\mathbf{H}_{\mathbf{x}j} = \begin{bmatrix} \mathbf{H}_{\mathbf{p}j}, & \mathbf{H}_{\mathbf{m}j} \end{bmatrix}$ where

$$\mathbf{H}_{\mathbf{p}j} = \left.\frac{\partial \mathbf{h}_j}{\partial \hat{\mathbf{x}}_p}\right|_{(\hat{\mathbf{x}}_p(k|k-1), p_i, \alpha_i)} = \begin{bmatrix} -c_i\cos(\alpha_i) & -c_i\sin(\alpha_i) & 0 \\ 0 & 0 & -1 \end{bmatrix}$$

and

$$\mathbf{H}_{\mathbf{m}j} = \left.\frac{\partial \mathbf{h}_j}{\partial \hat{\mathbf{x}}_m}\right|_{(\hat{\mathbf{x}}_p(k|k-1), p_i, \alpha_i)} = \begin{bmatrix} 0\ 0 \cdots c_i\ g_i \cdots 0\ 0 \\ 0\ 0 \cdots 0\ 1 \cdots 0\ 0 \end{bmatrix},$$

where $c_i = \text{sign}(Ci)$ and $g_i = c_i\hat{x}_r(k|k-1)\sin(\alpha_i) - c_i\hat{y}_r(k|k-1)\cos(\alpha_i)$. When observing the ith feature (a pair to the jth observation), the observation jacobian $\mathbf{H}_{\mathbf{m}j}$ is of dimension $2 \times 2n$ and is non-zero only at the location of the ith feature in the state vector $\hat{\mathbf{x}}_m(k|k-1)$. The observation jacobian for all the observations in $\mathbf{z}_M(k)$ is given by

$$\mathbf{H}_{\mathbf{x}} = \left[\mathbf{H}_{\mathbf{x}1}^T, \ldots, \mathbf{H}_{\mathbf{x}M}^T\right]^T.$$

The correction step is then defined as follows:

$$\hat{\mathbf{x}}(k|k) = \hat{\mathbf{x}}(k|k-1) + \mathbf{K}(\mathbf{z}_M(k) - \hat{\mathbf{z}}_M(k|k-1))$$
$$\mathbf{P}(k|k) = \mathbf{P}(k|k-1) - \mathbf{K}\mathbf{H}_{\mathbf{x}}\mathbf{P}(k|k-1)$$
$$\mathbf{K} = \mathbf{P}(k|k-1)\mathbf{H}_{\mathbf{x}}{}^T\left(\mathbf{H}_{\mathbf{x}}\mathbf{P}(k|k-1)\mathbf{H}_{\mathbf{x}}{}^T + \mathbf{R}\right)^{-1}, \quad (15)$$

where $\mathbf{R}$ is the observation covariance matrix

$$\mathbf{R} = \begin{bmatrix} \mathbf{R}_1 & 0 & \cdots & 0 \\ 0 & \mathbf{R}_2 & \cdots & \vdots \\ \vdots & \vdots & \ddots & \vdots \\ 0 & 0 & \cdots & \mathbf{R}_M \end{bmatrix}$$

composed of the covariance matrices $\mathbf{R}_j$ for each observation, which are estimated in Equation (8).

3.2.3. Correction step for new features

The observed line-feature parameters $\mathbf{z}_N(k) = [r_{M+1}, \psi_{M+1}, \ldots, r_{M+N}, \psi_{M+N}]$ not mapped yet are appended to the map $\hat{\mathbf{x}}_m(k|k-1)$. The observed line features $\mathbf{z}_N(k)$ with parameters r_f and ψ_f, $f = M+1, \ldots, M+N$ are transformed into the parameters $\hat{p}_f$ and $\hat{\alpha}_f$ expressed in the global coordinates (see Equation (13)) as follows:

$$Di = r_f - \hat{x}_r(k|k)\sin(\psi_f + \hat{\varphi}_r(k|k)) + \hat{y}_r(k|k)\cos(\psi_f + \hat{\varphi}_r(k|k))$$
$$\begin{bmatrix} \hat{p}_f \\ \hat{\alpha}_f \end{bmatrix} = \mathbf{g}(\hat{\mathbf{x}}_p(k|k), r_f, \psi_f) = \begin{bmatrix} |Di| \\ \psi_f + (\hat{\varphi}_r(k|k) - \frac{\pi}{2}) - (-0.5 \times \text{sign}(Di) + 0.5)\pi \end{bmatrix}.$$

The state vector $\hat{\mathbf{x}}(k|k)$ and the covariance matrix $\mathbf{P}(k|k)$ after adding new features become

$$\hat{\mathbf{x}}(k|k)^* = \left[\hat{\mathbf{x}}(k|k)^T, \mathbf{g}_{M+1}^T, \ldots, \mathbf{g}_{M+N}^T\right]^T$$
$$\mathbf{P}^*(k|k) = \begin{bmatrix} \mathbf{P}(k|k) & \mathbf{P}(k|k)\mathbf{G}_{\mathbf{x}}{}^T \\ \mathbf{G}_{\mathbf{x}}\mathbf{P}(k|k) & \mathbf{G}_{\mathbf{x}}\mathbf{P}(k|k)\mathbf{G}_{\mathbf{x}}{}^T + \mathbf{G}_{\mathbf{z}}\mathbf{R}\mathbf{G}_{\mathbf{z}}{}^T \end{bmatrix}, \quad (16)$$

where $\mathbf{G}_{\mathbf{x}}$ and $\mathbf{G}_{\mathbf{z}}$ are jacobian matrices, defined as follows:

$$\mathbf{G}_{\mathbf{x}} = \left[\mathbf{G}_{\mathbf{x}M+1}^T, \cdots, \mathbf{G}_{\mathbf{x}M+N}^T\right]^T$$
$$\mathbf{G}_{\mathbf{z}} = \begin{bmatrix} \mathbf{G}_{\mathbf{z}M+1} & 0 & \ldots & 0 \\ 0 & \mathbf{G}_{\mathbf{z}M+2} & \ldots & \vdots \\ \vdots & \vdots & \ddots & \vdots \\ 0 & 0 & \cdots & \mathbf{G}_{\mathbf{z}M+N} \end{bmatrix}$$

with

$$\mathbf{G}_{\mathbf{x}f} = \frac{\partial \mathbf{g}}{\partial \hat{\mathbf{x}}_p}\,|_{(\hat{\mathbf{x}}_p(k|k), r_f, \psi_f)} = \begin{bmatrix} -d_i\sin(\psi_f + \hat{\varphi}_r(k|k)) & d_i\cos(\psi_f + \hat{\varphi}_r(k|k)) & o_i \\ 0 & 0 & 1 \end{bmatrix}$$
$$\mathbf{G}_{\mathbf{z}f} = \left.\frac{\partial \mathbf{g}}{\partial [r_f, \psi_f]^T}\right|_{(\hat{\mathbf{x}}_p(k|k), r_f, \psi_f)} = \begin{bmatrix} d_i & o_i \\ 0 & 1 \end{bmatrix},$$

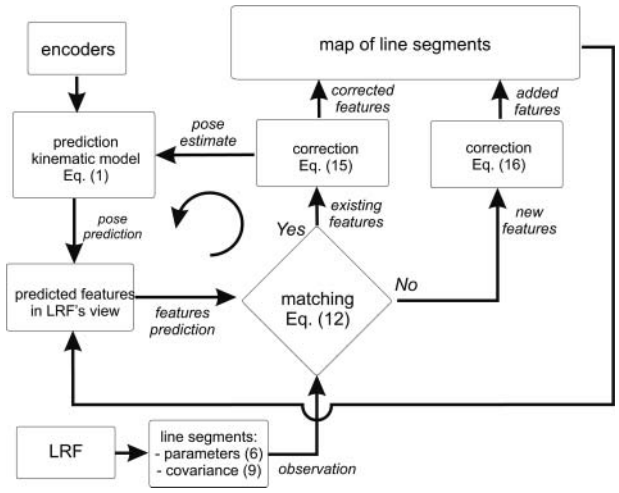

Figure 3. EKF-based SLAM for wheeled mobile robot.

where $d_i = \text{sign}\ (Di)$, $o_i = -d_i \hat{x}_r(k|k) \cos(\psi_f + \hat{\varphi}_r(k|k)) - d_i \hat{y}_r(k|k) \sin(\psi_f + \hat{\varphi}_r(k|k))$ and $\mathbf{R}$ is the observation covariance matrix

$$\mathbf{R} = \begin{bmatrix} \mathbf{R}_{M+1} & 0 & \cdots & 0 \\ 0 & \mathbf{R}_{M+2} & \cdots & \vdots \\ \vdots & \vdots & \ddots & \vdots \\ 0 & 0 & \cdots & \mathbf{R}_{M+N} \end{bmatrix}$$

composed of the covariance matrices $\mathbf{R}_j$ for each observation, which are estimated in Equation (8).

To avoid unreliable features appearing in the state vector, new features are first put in a trial list and added to the state vector after they have been seen a predefined number of times in some time period (Dissanayake, Newman, Clark, Durrant-Whyte, and Csorba 2001). The possible occurrence of multiple features in the state vector, which represent the same line in the environment, can be fused together by periodically validating the state vector (Garulli et al. 2005).

A flow chart of the presented SLAM algorithm is shown in Figure 3.

In the proposed SLAM the accuracy of localisation and mapping depends on the accuracy of the line-feature parameters estimation from the measured LRF's reflection points. An important issue in the line segment landmarks is that error in perpendicular distance var(r) varies significantly in case of small changes in the line slope if the robot is far away from the line. In a situation when the observed objects are far and their line segments are estimated from a smaller number of LRF's points the estimated line parameters have higher variances which consequentially lowers the localisation accuracy. According to Equation (9) the variance var(r) of the parameter r mainly depends on the variance var(k_l) and on K_{rk} (10) which defines the sensitivity of the line parameter r according to the slope of the line k_l.

var(k_l) in Equation (7) depends on vertical-error var($y(j)$) which is influenced by LRF's angular and distance measurement noise. The shape of function K_{rk} with respect to the parameters of the line segment is given in Figure 4. According to Equation (10) K_{rk} is larger if c_l is large (i.e.,

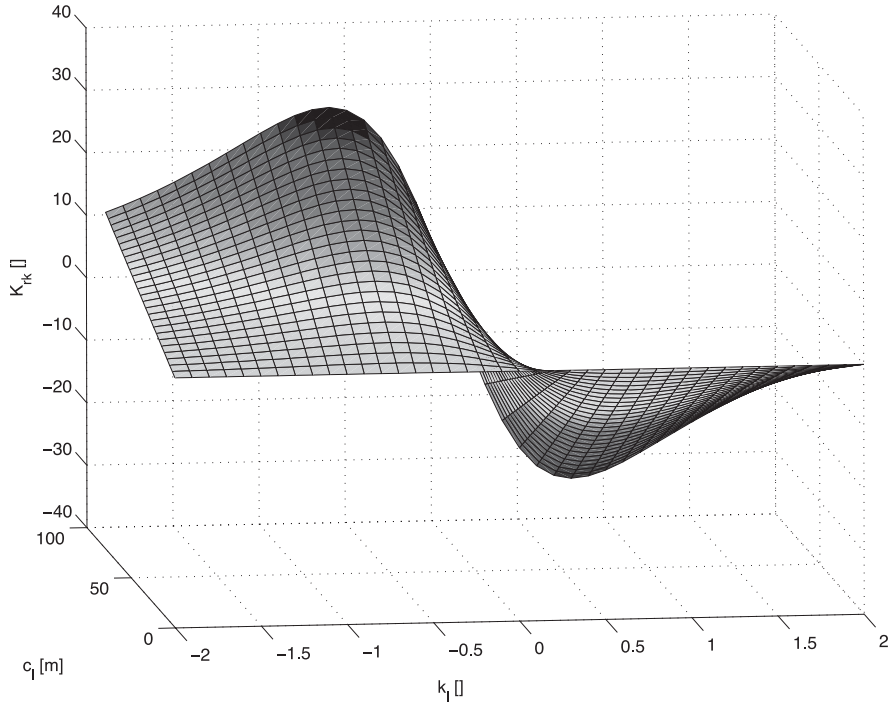

Figure 4. Uncertainty propagation function K_{rk} with respect to k_l and c_l.

robot is far from the environment line) and gets maximum at (see Equation (10))

$$\left.\frac{\partial K_{rk}}{\partial k_l}\right|_{c_l=\text{const}} = 0 \implies ({k_l}^2+1)^{-\frac{3}{2}} - 3{k_l}^2({k_l}^2+1)^{-\frac{5}{2}} = 0$$

$$\implies |k_l| = \frac{\sqrt{2}}{2}. \tag{17}$$

This means that when observing the far-away line with the slope $|k_l| = \frac{\sqrt{2}}{2}$ the small variations of k_l are magnified by a factor $|K_{rk}| = 0.385|c_l|$ to deviations of r. In this special case a larger variance of parameter r lowers the correction gain in EKF (**K** in Equation (15)) and increases variances of the estimated robot pose. Because the line parameter r depends on the robot pose in the environment also the variance var(r) depends on the robot pose. As already mentioned this worst case scenario could happen when the line is estimated from a smaller number of points. However, the estimated uncertainties are still in tolerance band which enables a good localisation of the robot.

To support the above statements the effect of the proposed line segment uncertainties to the uncertainties of the estimated robot pose using EKF is analysed. As seen from Equation (7) covariance matrix of estimated line parameters k_l, c_l are dependant on a set of points for line parameters estimation this is on their location according to robot coordinate frame. To simplify this analysis let us suppose that the estimated line parameters covariance matrix **Z** in Equation (7) are constant for the arbitrary observed line in the environment with the variances set as follows $\text{var}(k_l) = 2.5 \times 10^{-3}$, $\text{var}(c_l) = 0.1 \times 10^{-3}\,\text{m}^2$ and $\text{cov}(c_l, k_l) = 0\,\text{m}$, respectively. In the analysis the robot is located at $x_r = 0\,\text{m}$, $y_r = 0\,\text{m}$ and $\varphi_r = 0\,^\circ$ and is not moving. It observes one line segment with parameters k_l and c_l. Initial state-estimation error uncertainty is set to $\text{var}(x_r) = 0.1\,\text{m}^2$, $\text{var}(y_r) = 0.1\,\text{m}^2$ and $\text{var}(\varphi_r) = 0.1\,\text{rad}^2$ while the line parameters in global map (state vector $\hat{\mathbf{x}}_m(k|k-1)$) have zero uncertainty. In the analysis the variance of the normal line parameters is calculated using Equation (9) and their dependence to the parameters k_l and c_l is given in Figure 5.

Where it can be seen that maximum uncertainty of var(r) is located at $k_l = \pm\frac{\sqrt{2}}{2}$ as already calculated in Equation (17). Then by considering correction step (Equations (13)–(15)) the new robot pose uncertainty dependent on the line parameters k_l and c_l is calculated as shown in Figure 6.

Variances var(x_r) and var(y_r) in Figure 6 increase with c_l. At $k_l = 0$ the variance var(x_r) is the highest because robot orientation ($\varphi_r = 0$) and the observed line are aligned with the x axis while on the contrary the variance var(y_r) is the lowest.

In Figure 7 the distance uncertainty $\text{var}(dist) = \text{var}(x_r) + \text{var}(y_r)$ from the true robot position ($x_r = 0\,\text{m}$, $y_r = 0\,\text{m}$) is shown where again the maximum uncertainty is located at $k_l = \pm\frac{\sqrt{2}}{2}$ and increases with higher values of c_l.

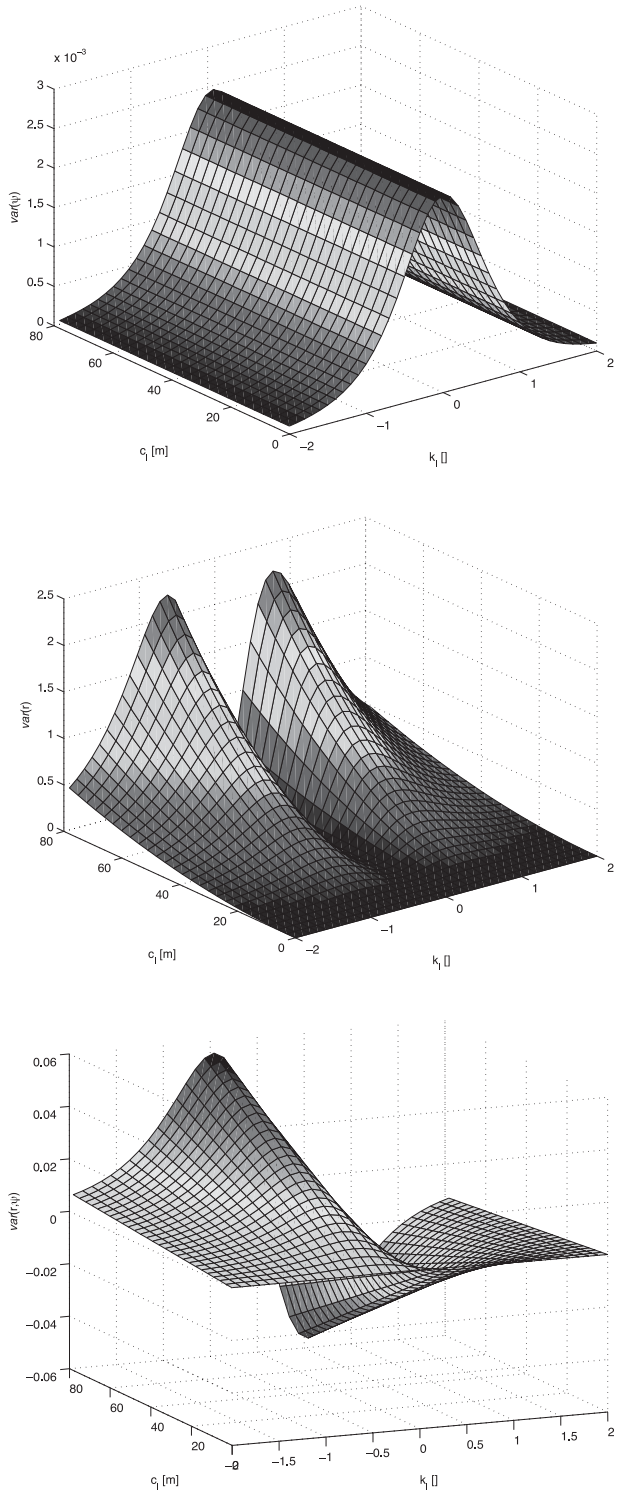

Figure 5. Uncertainty var (ψ), var(r) and var (r, ψ) with respect to k_l and c_l.

At low values of c_l (line is close to the robot) distance uncertainty becomes low according to Equation (11) and assumption that var(k_l) and var(c_l) are constant irrespective of where the line is according to the robot. It should be noted that in practice (see Equation (7)) the estimated uncertainty

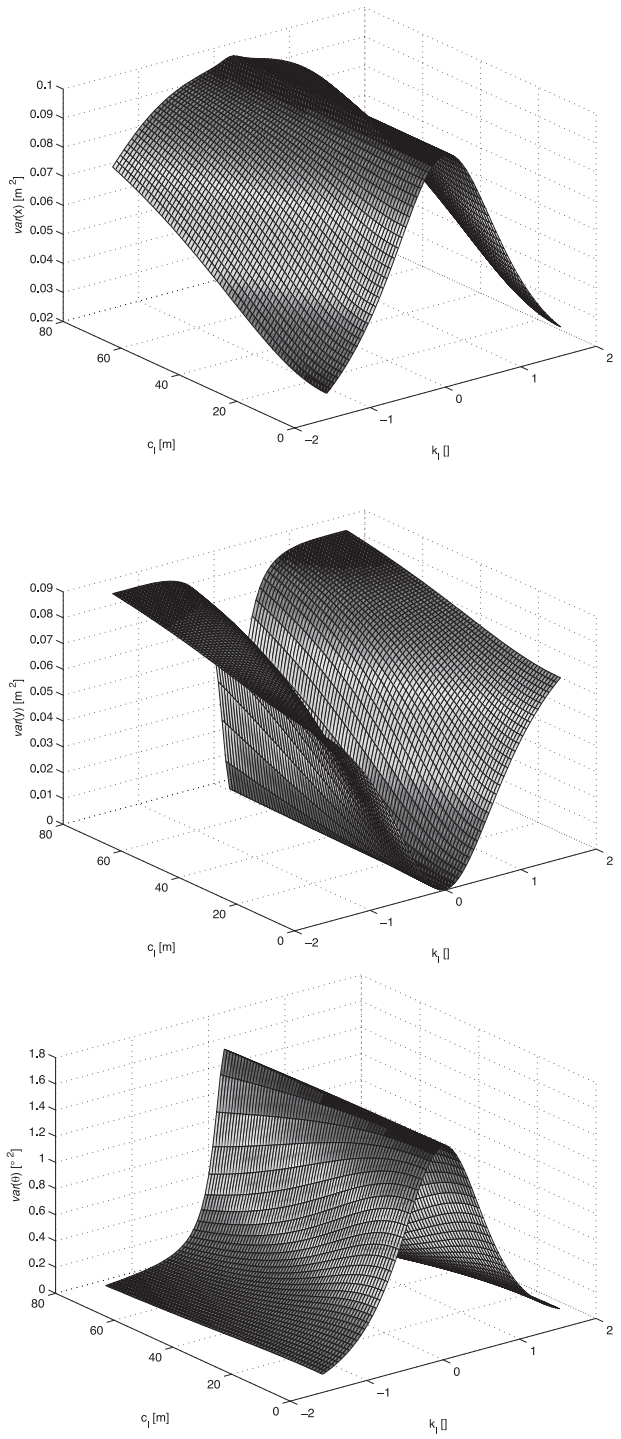

Figure 6. Uncertainty var(x_r), var(y_r) and var(φ_r) with respect to k_l and c_l.

of line parameters k_l and c_l is a bit higher if the line is close to the robot. This happens because LRF has quite constant noise when measuring distance to either closer of farther reflection points. If the line segment is closer to the robot and estimated from the same number of the line segment points then it is shorter. The measured reflection points are due to the shorter line segment relatively more scattered around the true line and the estimated covariances by Equation (7) become higher.

3.3. *Validation of estimated observation uncertainty*

The appropriate operation of EKF depends on the correct assumption of uncertainties that influence state estimation process (Borges and Aldon 2003; Sakai and Kuroda 2010). In the following some directions and the validation of the proposed method for the estimation of observation uncertainty are given.

3.3.1. *Note on stability and convergence of EKF*

According to Julier (1997) a consistent estimate of covariance matrix $\mathbf{P}(k|k)$ in correction step is required to achieve stable operation of EKF. The condition to obtain conservative estimate $\mathbf{P}(k|k)$ is $\mathbf{P}(k|k) - \overline{\mathbf{P}}(k|k) \geq 0$, where $\overline{\mathbf{P}}(k|k)$ is true covariance matrix in the correction step. A sufficient condition to ensure positive definiteness of the difference $\mathbf{P}(k|k) - \overline{\mathbf{P}}(k|k)$ is consistence of the prediction covariance $\mathbf{P}(k|k-1)$ and the observation covariance $\mathbf{R}(k)$

$$\begin{gathered}\mathbf{P}(k|k-1) - \overline{\mathbf{P}}(k|k-1) \geq 0 \\ \mathbf{R}(k) - \overline{\mathbf{R}}(k) \geq 0,\end{gathered}$$

where $\overline{\mathbf{P}}(k|k-1)$ is true prediction covariance and $\overline{\mathbf{R}}$ is true observation covariance. The first condition requires consistent prediction $\mathbf{P}(k|k-1)$ which is achieved by setting the input covariance matrix (3). The second condition requires that the estimated observation noise exceeds that of the true system.

The convergence of EKF explains how fast the estimated states approach to the true states. In stable EKF operation the convergence is faster if the estimated noise covariances are closer to the true ones. Small estimated observation-noise covariance causes high gain matrix (15) in the correction step of EKF. However, the estimated noise (input and observation) must not be lower than the true noise to obtain stable EKF operation. Additionally, the input $\mathbf{Q}(k)$ and observation $\mathbf{R}(k)$ matrices must be properly balanced. If not balanced correctly, then the observation errors may incorrectly influence the state estimation ($\mathbf{Q}(k) - \bar{\mathbf{Q}}(k) \gg 0$, $\mathbf{R}(k) - \bar{\mathbf{R}}(k) \geq 0$) or the state estimation may become insensitive to the observation residuals ($\mathbf{Q}(k) - \bar{\mathbf{Q}}(k) \geq 0$, $\mathbf{R}(k) - \bar{\mathbf{R}}(k) \gg 0$).

3.3.2. *Statistical comparison*

The appropriate observation covariance $\mathbf{R}(k)$ needs to be estimated to achieve good performance regarding stability and convergence as stated above. Additionally, accurate

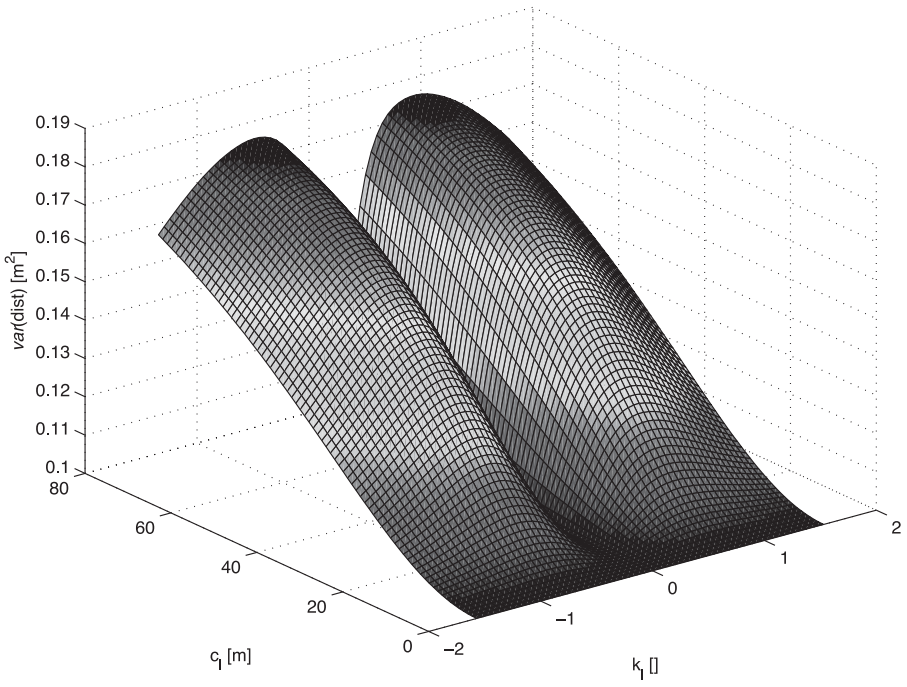

Figure 7. Distance uncertainty var(*dist*) with respect to k_l and c_l.

estimation of observation covariance also enables better matching results between the observed features and the features in global map which is done using Mahalanobis distance (12). Therefore, an appropriate estimation method is required.

In Section 2 the method for estimating the observation covariance is given (Equations (5)–(10)) using LSQ and linearisation of the nonlinear dependency between parameters of explicit and normal line Equation (6).

Here the comparison of the proposed method using linearisation (LIN) is made to the method using unscented transform (UT) which is known to give good estimation results in case of nonlinearities (Hartikainen et al. 2011). UT is used to approximate the observation covariance where the explicit line parameters uncertainty propagates through nonlinear relation (6) to the uncertainty of line parameters in normal form. This could give a more accurate estimate than the error propagation via first-order Taylor series expansion.

Input information to the UT method is a current estimate of explicit line parameters $\hat{\theta} = [\hat{k}_l, \hat{c}_l]^T$ (see Equation (5)) and its covariance matrix $\mathbf{Z}$ (see Equation (7)). The observation covariance can be calculated using UT, as shown in Hartikainen et al. (2011), as follows:

- Five ($2n + 1$, n is the dimension of $\hat{\theta}$) sigma points $\mathbf{X}$ are calculated, one is the current estimate $\hat{\theta}$ and the other four are obtained by perturbation of the first in the direction of the principal component axes of $\mathbf{Z}$

$$\mathbf{X} = \begin{bmatrix} \hat{\theta} & \hat{\theta} & \hat{\theta} & \hat{\theta} & \hat{\theta} \end{bmatrix} + \sqrt{c} \begin{bmatrix} \mathbf{0} & \sqrt{\mathbf{Z}} & -\sqrt{\mathbf{Z}} \end{bmatrix},$$

where $\sqrt{\mathbf{Z}}$ is obtained using Cholesky factorisation and $c = \alpha^2(n + \kappa)$ is scaling parameter. The positive constants α, β and κ in the comparison are $\alpha = 0.01$, $\beta = 2$ and $\kappa = 1$ (for more details see Sakai and Kuroda 2010; Hartikainen et al. 2011).

- Sigma points $\mathbf{X}$ are propagated through nonlinearity $\mathbf{g}$ defined in Equation (6)

$$\mathbf{Y} = \mathbf{g}(\mathbf{X}),$$

where function $\mathbf{g}(\cdot)$ is applied to each column of $\mathbf{X}$ separately.

- Estimate of observation covariance matrix is then defined as

$$\mathbf{R}_{UT} = \mathbf{Y}\mathbf{W}\mathbf{Y}^T, \tag{18}$$

where $\mathbf{W}$ is weight matrix, defines as

$$\begin{aligned} \mathbf{W} &= (\mathbf{I} - [\mathbf{w}_m \cdots \mathbf{w}_m]) \operatorname{diag}\left(W_c^{(0)} \cdots W_c^{(2n)}\right) \\ &\quad (\mathbf{I} - [\mathbf{w}_m \cdots \mathbf{w}_m])^T \\ \mathbf{w}_m &= \left[W_m^{(0)} \cdots W_m^{(2n)}\right] \\ W_m^{(0)} &= \lambda/(n+\lambda) \\ W_c^{(0)} &= \lambda/(n+\lambda) + (1 - \alpha^2 + \beta) \\ W_m^{(i)} &= W_c^{(i)} = 1/\left(2(n+\lambda)\right), \quad i = 1, \ldots, 2n \end{aligned}$$

where $\lambda = \alpha^2(n + \kappa) - n$.

Table 1 Three environment line segments, which correspond to $n = 36$ LRF's points.

$r_{e1} = 2m$,	$\psi_{e1} = 90^\circ$,	$\theta_s(j)$: $60^\circ, 61^\circ, \ldots, 95^\circ$
$r_{e2} = 50m$,	$\psi_{e2} = 130^\circ$,	$\theta_s(j)$: $80^\circ, 81^\circ, \ldots, 115^\circ$
$r_{e3} = 10m$,	$\psi_{e3} = 170^\circ$,	$\theta_s(j)$: $97^\circ, 98^\circ, \ldots, 132^\circ$

The comparison of both methods (LIN and UT) for estimating the covariance matrix is done using statistical analysis. Three different environment line segments are simulated. They are defined by normal line parameters (r_{ei}, ψ_{ei}; $i = 1, 2, 3$) (Tables 1 and 2) and laser-beam angels $\theta_s(j)$, at 1° resolution or $n = 36$ points for each line segment.

The LRF's noise is approximated using normal distribution with zero mean and standard deviations for distance measurement error $\sigma_d = 30$ mm and for laser-beam error $\sigma_\theta = 0.017rad$.

Each line experiment is repeated many times (e.g., $N_{tr} = 10,\ 000$). The line parameters r_u and ψ_u ($u = 1, \ldots, N_{tr}$) calculated by LSQ (5) and (6) slightly differ in each experiment due to the LRF's noise. The reference standard deviation of both line parameters and the covariance between them are calculated for both methods by

$$\sigma_{r_u} = \sqrt{\frac{1}{N_{tr}} \sum_{u=1}^{N_{tr}} (r_u - r_{ei})^2},$$

$$\sigma_{\psi_u} = \sqrt{\frac{1}{N_{tr}} \sum_{u=1}^{N_{tr}} (\psi_u - \psi_{ei})^2},$$

$$\text{cov}\ (r_u,\ \psi_u) = \frac{1}{N_{tr}} \sum_{u=1}^{N_{tr}} (r_u - r_{ei}) * (\psi_u - \psi_{ei});$$

$$i = 1, 2, 3, \tag{19}$$

and are shown in Table 2. They are used for comparison of already described methods for estimation of the variances and covariance.

Firstly, the standard deviations $\sigma_r = \sqrt{\text{var}(r)}$, $\sigma_\psi = \sqrt{\text{var}(\psi)}$ and the covariance $covar(r, \psi)$ are calculated with the method resulting from LSQ and linearisation (9). Here, the vertical-error variance $\text{var}(\mathbf{y}(j))$ (7) is calculated from the LRF's points, as shown in Equation (7). If this variance is estimated from a very small (e.g., 5) number of line-segment points, the estimation is not very accurate. If an accurate variance of the LRF's distance-measurement error $\sigma_{d_j}^2$ and variance of the laser-beam angle error $\sigma_{\theta_j}^2$ are given from a LRF's noise model, a better estimation of the vertical-error variance $\text{var}(\mathbf{y}(j))$ can be calculated (in Table 2 this is marked with a priori prefix).

In Table 2 the results of the experiments are shown where the standard deviations and the covariance of the line parameters r and ψ were calculated with the method resulting from linearisation as $\sigma_r = \sqrt{\text{var}(r)}$, $\sigma_\psi = \sqrt{\text{var}(\psi)}$ and cov (r, ψ) (9) and with the method resulting from the UT (18) as $\sigma_r = \sqrt{\mathbf{R}^*_{UT}(1,1)}$, $\sigma_\psi = \sqrt{\mathbf{R}^*_{UT}(2,2)}$ and $\text{cov}(r,\ \psi) = \mathbf{R}^*_{UT}(2,1)$. All three environment line segments in Table 1 are considered. Due to LRF's noise ($\sigma_{d_j}^2$ and $\sigma_{\theta_j}^2$) these two variances and the covariance as well as the reference variances σ_r and σ_ψ and the covariance $\text{cov}(r, \psi)$ are different in each experiment. Therefore, the mean and standard deviation of all ($N_{tr} = 10,\ 000$) calculated standard deviations are shown in Table 2. Standard deviations $\text{std}(\sigma_r)$, $\text{std}(\sigma_\psi)$ and $\text{std}(\text{cov}(r, \psi))$ are calculated according to means $\text{mean}(\sigma_r)$, $\text{mean}(\sigma_\psi)$ and $\text{mean}(\text{cov}(r, \psi))$, respectively. mean(·) and std(·) of the variances σ_r and σ_ψ and covariances $\text{cov}(r, \psi)$ in Table 2 refer to the case where $\text{var}(\mathbf{y}(j))$ is estimated from the LRF points during

Table 2 Comparison of the accuracy of the covariance estimation method using linearisation (LIN) and unscented transform (UT), where three different environment line segments (r_{ei}, ψ_{ei}; $i = 1, 2, 3$) are simulated.

	r_{e1}, ψ_{e1}		r_{e2}, ψ_{e2}		r_{e3}, ψ_{e3}	
	LIN	UT	LIN	UT	LIN	UT
σ_{r_u}	7.74	7.74	26.98	26.98	15.28	15.28
$\text{mean}(\sigma_r)$	7.30	7.30	28.70	29.11	14.48	14.58
$\text{std}(\sigma_r)$	0.92	0.92	4.07	4.01	1.99	1.97
a priori:$\text{mean}(\sigma_r)$	7.45	7.46	29.52	26.91	14.83	14.93
a priori:$\text{std}(\sigma_r)$	0.20	0.20	0.053	0.052	0.014	0.014
σ_{ψ_u}	0.0122	0.0122	9.2×10^{-4}	9.2×10^{-4}	0.001	0.001
$\text{mean}(\sigma_\psi)$	0.0121	0.0121	8.0×10^{-4}	8.3×10^{-4}	8.1×10^{-4}	8.4×10^{-4}
$std(\sigma_\psi)$	0.0015	0.0015	1×10^{-4}	1×10^{-4}	1×10^{-4}	1×10^{-4}
a priori:$\text{mean}(\sigma_\psi)$	0.0123	0.0123	8.2×10^{-4}	8.5×10^{-4}	8.3×10^{-4}	8.7×10^{-4}
a priori:$\text{std}(\sigma_\psi)$	8×10^{-5}	8×10^{-5}	3×10^{-7}	3×10^{-7}	1.7×10^{-6}	1.6×10^{-6}
$\text{cov}(r_u, \psi_u)$	−0.074	−0.074	−0.023	−0.023	−0.014	−0.014
$\text{mean}(\text{cov}(r, \psi))$	−0.068	−0.068	−0.022	−0.021	−0.011	−0.011
$\text{std}(\text{cov}(r,\ \psi))$	0.017	0.017	0.006	0.006	0.003	0.003
a priori:$\text{mean}(\text{cov}(r,\ \psi))$	−0.070	−0.070	−0.022	−0.021	−0.011	−0.011
a priori:$\text{std}(\text{cov}(r,\ \psi))$	0.003	0.003	5×10^{-5}	5×10^{-5}	4×10^{-5}	4×10^{-5}

each experiment. a priori:mean(·) and a priori:std(·) of the variances σ_r and σ_ψ and covariances cov(r, ψ) in Table 2 refer to the case where var($\mathbf{y}(j)$) is estimated from the a priori known variances of the LRF's noise model $\sigma^2_{d_j}$ and $\sigma^2_{\theta_j}$. Accuracy of the estimated standard deviations and the covariance (when var($\mathbf{y}(j)$) is estimated from points) is depended on the number of line-segment points (less accurate at lower number of points), therefore, a more accurate estimates are obtained if LRF's noise model is a priori given. In the experiments a priori known variances $\sigma^2_{d_j}$ and $\sigma^2_{\theta_j}$ were set to the true variances $(30\,\text{mm})^2$ and $(0.0017\,\text{rad})^2$, respectively.

As seen from Table 2 both methods are close to the reference standard deviation and covariance. UT method does not bring any noticeable advantage over the proposed method using linearisation (LIN) which means that uncertainty propagation through nonlinear relation (6) does not play an important role here and can be approximated by less computational expensive linearisation (8). The calculation of Cholesky factorisation to obtain square root of the covariance matrix $\mathbf{Z}$ is an iterative process and requires a much higher computational burden than linearisation (Sakai and Kuroda 2010). By measuring the elapsed time for line experiment a rough estimate of computational complexity of the proposed LIN method regarding the UT method is estimated. For $N_{tr} = 10,000$ times repeated line experiment LIN method takes $1.7s$ on a personal computer (2 Quad CPU, 2.66 GHz, implementation in Matlab) while UT method takes $3.3s$ which is 94% more. UT method may become beneficial only if the noise level of the applied LRF SickLMS200 would be much higher than currently estimated in the experiments.

4. Experimental results

The proposed SLAM algorithm was experimentally validated on the mobile robot Pioneer 3-AT. In the experiment the mobile robot was driven by setting constant angular velocities to its wheels $\omega_R(k) = 2.7\,\text{rad/s}$ and $\omega_L(k) = 1.9\,\text{rad/s}$, $k = 1, \ldots, 500$ causing the robot to circle in the environment with a translational speed of 0.37 m/s. The robot scans the environment and makes map updates at a frequency of 10 *Hz*. The robot's initial pose was set to $\hat{\mathbf{x}}_p(1|1) = [0, -1, 0]^T$ with an initial uncertainty $\text{std}(\hat{x}_r(1|1)) = \text{std}(\hat{y}_r(1|1)) = 1\,\text{cm}$ and $\text{std}(\hat{\varphi}_r(1|1)) = 0.01\,\text{rad}$.

Due to disturbances such as, the input noise, the slipping of the wheels and similar the robot's path is not a perfect circle, as seen in Figure 11. The input-noise covariance $\mathbf{Q}(k)$ is estimated as proposed in Equation (3), where $\delta = 0.1$. The observation covariance matrix $\mathbf{R}$ is estimated for each identified line feature in the LRF's scan using the least-squares method, as described in Equations (7)–(10).

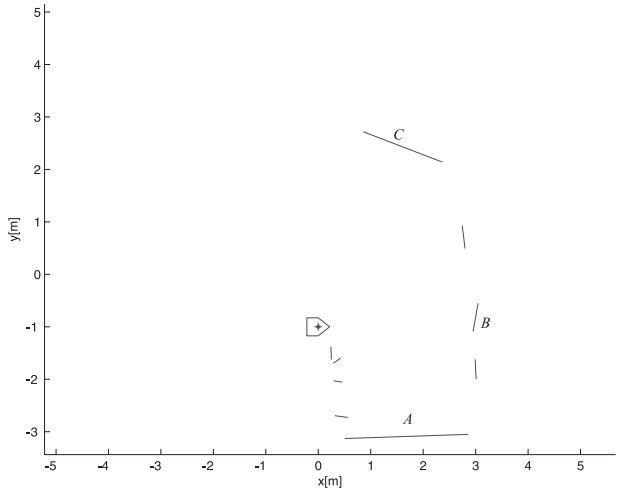

Figure 8. Robot pose and mapped line features of the environment at time $k = 2$.

The consecutive maps of the environment and the robot path at time instants $k = 2$, 50, 300, 500 are shown in Figures 8–11.

The map of the identified line features evolves over time. During the first observation, the features have a high uncertainty, which is then reduced with new observations.

Figures 12–14 show the estimated line parameters and their uncertainty area for three different line features marked in Figures 8–11 as A, B and C, respectively. The feature A in Figure 12 has $\alpha \doteq -\pi/2$, the feature B in Figure 13 has $\alpha \doteq 0$ and the feature C in Figure 14 has $\alpha \doteq \pi/3$. The uncertainty is defined by three standard deviations (95% probability) and shown for the time course k. It can be seen that the features' uncertainty decreases and is at the best bounded with the initial uncertainty of the robot pose. The uncertainty of the feature B in Figure 13 is high, according

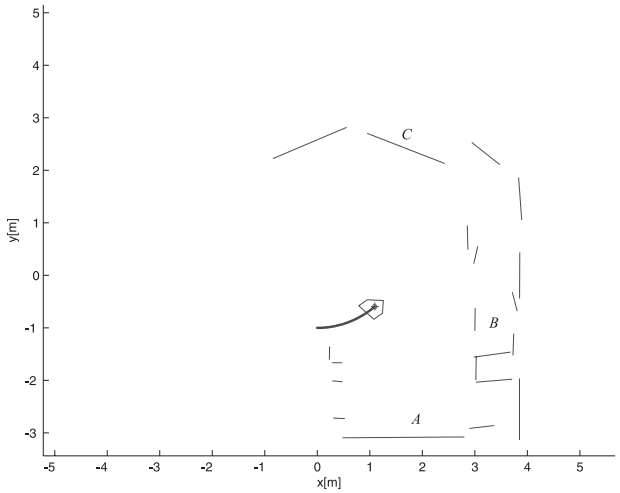

Figure 9. Robot pose and mapped line features of the environment at time $k = 50$.

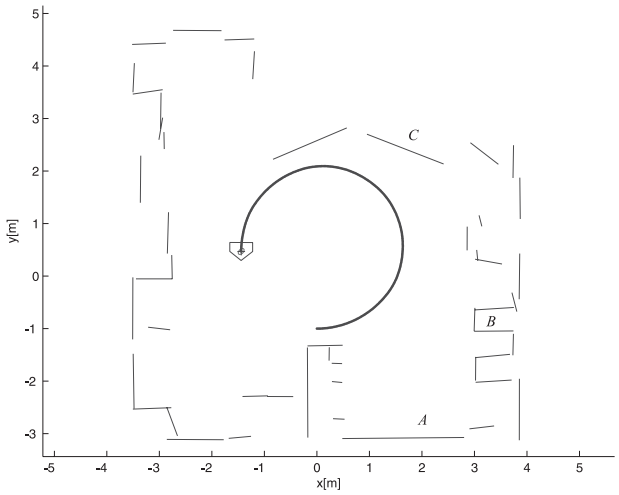

Figure 10. Robot pose and mapped line features of the environment at time $k = 300$.

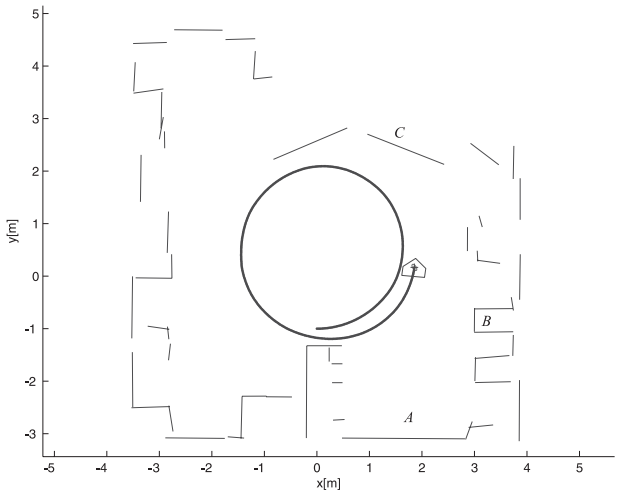

Figure 11. Robot pose and mapped line features of the environment at time $k = 500$.

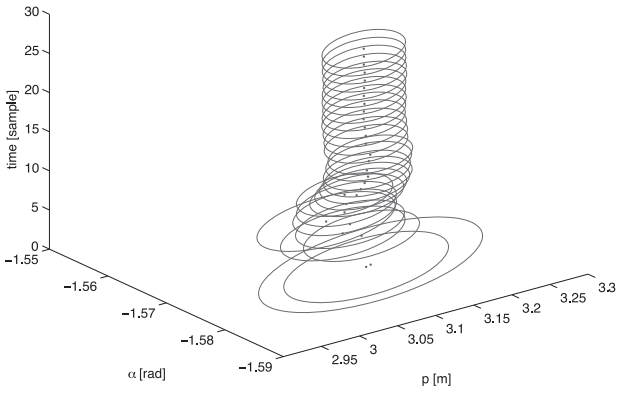

Figure 12. Estimated line parameters of feature A and the 95% probability area of the estimate for the time course.

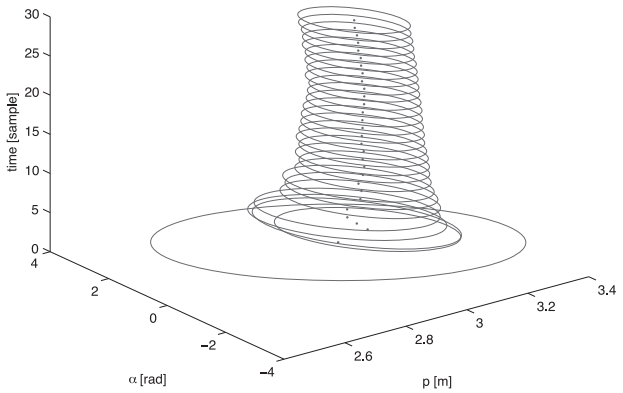

Figure 13. Estimated line parameters of feature B and the 95% probability area of the estimate for the time course.

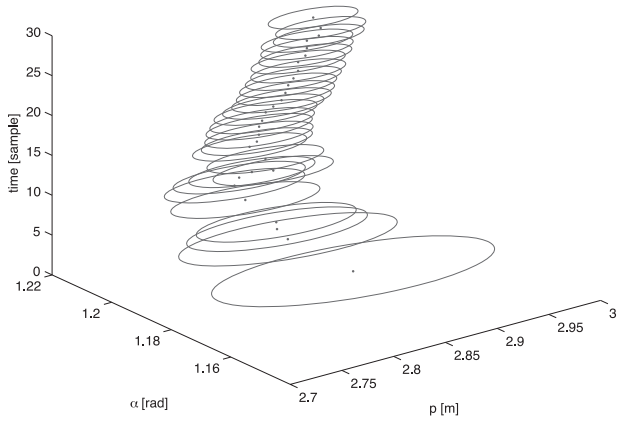

Figure 14. Estimated line parameters of feature C and the 95% probability area of the estimate for the time course.

to the uncertainty of the feature A in Figure 12, because the line is estimated from a smaller number of LRF's reflection points.

According to Section 3.3, the proposed SLAM approach is stable if estimated covariances $P(k|k)$ in the correction step are higher or at least equal to the true one. To obtain a faster convergence of the estimated parameters the covariances should be close to the true values and must not be smaller than the true covariances to have stable EKF estimation. In Table 2 the statistical analysis of the proposed covariance estimation method accuracy is made. This analysis shows that estimated covariances are close to the true covariances. However, to assure stability of EKF the estimated covariances need to be also consistent. According to performed analysis stable operation is guaranteed if, for example, the obtained estimated covariances are increased for approximately 10% which assures that estimated covariances are still close and higher than the true covariances.

The experimental analysis of the SLAM algorithm operation is shown in Figure 15. The estimated robot pose variances are shown for the proposed output-noise

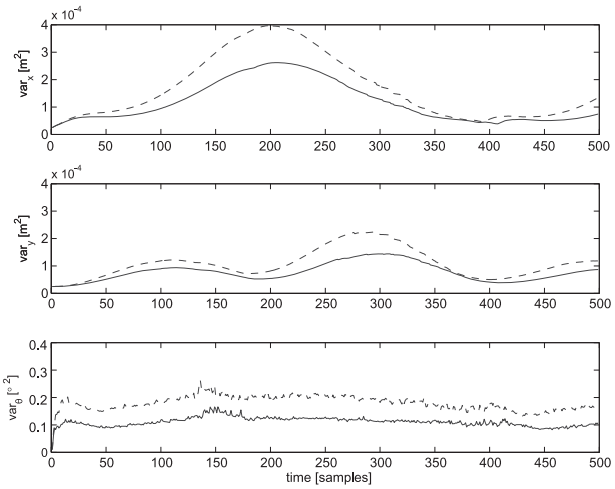

Figure 15. Estimated variances of robot position and orientation. Comparison for the proposed estimated output-noise covariances (solid line) and for constant conservatively set output-noise covariances (dashed line).

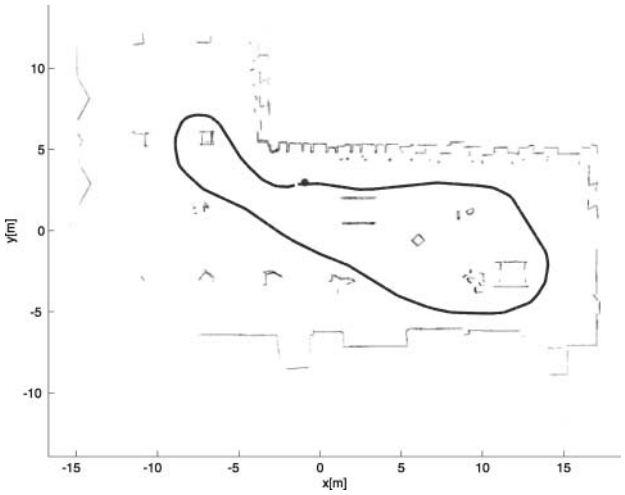

Figure 17. Estimated robot trajectory and environment map by the SLAM implemented in the original Pioneer 3-AT software.

covariance matrix estimation and for the constant conservatively set output-noise covariance matrix. The constant conservative output covariance matrix is selected by experiments so that a stable SLAM operation is achieved. As stated in Subsection 3.3, the consistent estimate of input and observation covariance must not be optimistic, therefore, the worst case scenario with the highest estimated uncertainties is selected to tune the constant output covariance matrix. It is obvious that the proposed output-covariances estimation scheme results in smaller pose covariances. In average up to 20% lower pose covariances are achieved, which results in faster convergence of the SLAM algorithm.

In the following a comparison of the proposed SLAM algorithm and SLAM algorithm implemented in the original Pioneer 3-AT software Mapper3 from MobileRobots Inc. (see MobileRobots 2009) is given in Figures 16 and 17. The Pioneer 3-AT SLAM software uses Monte-Carlo based approach. The software is reliable and very often used and has been verified by many researchers; therefore, the comparison makes sense.

Both SLAM algorithms were performed in the same experiment and initialised with the same initial pose estimate. The proposed SLAM is running in real time while the SLAM implemented in Mapper3 programme only collects

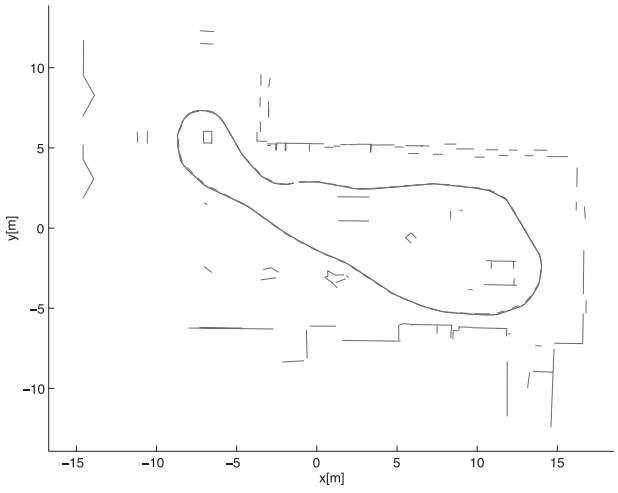

Figure 16. Estimated robot trajectory (–) and environment map by the proposed SLAM. Comparison to the estimated trajectory by the SLAM implemented in the original Pioneer 3-AT software (- -).

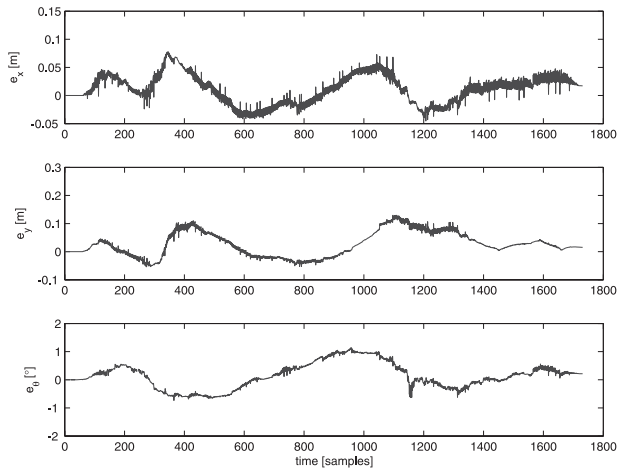

Figure 18. Difference between the pose estimates from the proposed SLAM and the SLAM implemented in the original Pioneer 3-AT software.

data in real time and then implements SLAM algorithm offline.

Note that the pose obtained by the Pioneer 3-AT localisation software is approximate and can even be less accurate than the pose of the proposed SLAM. As seen from Figures 16 and 17 the results (estimated trajectory and obtained map) are very similar. The closer difference between the pose estimates of both SLAM approaches is given in Figure 18. The difference between them is small (10 cm in position and 1° in orientation) therefore both SLAM are accurate.

The absolute accuracy of the estimated robot pose is tested for the final pose only, i.e. where the robot stops. The robot's position and orientation error in the final pose, estimated from more experiments, is evaluated as being approximately 4 cm and 0.7° for the proposed SLAM and 6 cm and 0.8° for the SLAM implemented in Pioneer 3-AT software, respectively.

5. Conclusion

In this paper a SLAM based on the EKF for a mobile robot navigating in indoor environment is presented. The robot is equipped with incremental encoders and LRF sensors, used to estimate its pose and to map the environment with a line-based representation. To achieve good convergence of the pose and environment map estimates (given in the system states of the EKF) methods for estimating the input and output covariance matrices are presented. Their realistic approximation contributes to the lower uncertainties of the estimated system states compared to the usual case where the covariances need to be set conservatively with higher values. The proposed observation covariance matrix estimation method which uses linearisation of nonlinear noise propagation function is statistically compared to the unscented transform which is known to give good estimation results in case of nonlinearities. It is established that unscented transform (UT) method does not bring any noticeable advantage over the proposed method using linearisation which means that nonlinearity of noise propagation function can be approximated by a less computationally expensive linearisation. UT method may become beneficial only if the applied LRF's noise level would be much higher. The limitation of the proposed SLAM approach is the use of line-based features only, which could make the operation in unstructured outdoor environments less reliable. The further developments would therefore focus on a system upgrade with a vision sensor. The proposed SLAM could also be upgraded with obstacle avoidance and path planning capabilities to achieve fully autonomous SLAM mission. Due to good convergence properties obtained by the simultaneous estimates of uncertainties the proposed methods will also be applied to other mobile systems.

Notes on contributors

Gregor Klančar received BSc and PhD degrees in electrical engineering from the University of Ljubljana, Slovenia in 1999 and 2003 respectively. He is currently employed as an assistant professor at the Faculty of Electrical Engineering at the University of Ljubljana. His research interest includes the area of fault diagnosis methods, the mobile robotics area and the area of control and supervision of multiagent systems. His work on mobile robotics area focuses on motion control, trajectory tracking, localisation, agent-based behaviour systems and strategies for enabling cooperative behaviours of agents in some group mission.

Luka Teslić received the BSc degree in electrical engineering from the University of Ljubljana, Slovenia, in 2006. In 2011 he received a PhD degree in mobile robotics at the University of Ljubljana. His research interests include mobile robot localisation and map building and fuzzy system identification. Currently, his interest is focused to control systems in space applications.

Igor Škrjanc received BSc, MSc and PhD degrees in electrical engineering, in 1988, 1991 and 1996, respectively, at the Faculty of Electrical and Computer Engineering, University of Ljubljana, Slovenia. He is currently full professor on the same faculty. His main research areas are adaptive, predictive, fuzzy and fuzzy adaptive control systems. Recently, he is working in the field of autonomous mobile systems in sense of localisation, direct visual control and trajectory tracking control. He was also involved in several European projects and bilateral projects. In 2008 he received the most important Slovenian research award for his work in the area of intelligent modelling and control – Zois award. In year 2009 he obtained a Humboldt research award for research at University of Siegen.

References

Anousaki, G.C., and Kyriakopoulos, K.J. (2007), 'Simultaneous Localization and Map Building of Skid-steered Robots', *IEEE Robotics and Automation Magazine*, 14(1), 79–89.

Bailey, T., and Durrant-Whyte, H. (2006), 'Simultaneous Localization and Mapping (SLAM): Part II', *IEEE Robotics & Automation Magazine*, 13(3), 108–117.

Baltzakis, H., and Trahanias, P. (2003), 'A Hybrid Framework for Mobile Robot Localization: Formulation Using Switching State-space Models', *Autonomous Robots*, 15(2), 169–191.

Borges, G.A., and Aldon, M.J. (2003), 'Robustified Estimation Algorithms for Mobile Robot Localization Based on Geometrical Environment Maps', *Robotics and Autonomous Systems*, 45, 131–159.

Borges, G.A., and Aldon, M.J. (2004), 'Line Extraction in 2D Range Images for Mobile Robotics', *Journal of Intelligent and Robotic Systems*, 40(3), 267–297.

Bošnak, M., Matko, D., and Blažič, S. (2012), 'Quadrocopter Control Using an On-board Video System With Off-board Processing', *Robotics and Autonomous Systems*, 60(4), 657–667.

Crowley, J.L., Wallner, F., and Schiele, B. (1998), 'Position Estimation Using Principal Components of Range Data', *Robotics and Autonomous Systems*, 23(4), 267–276.

Dakulović, M., and Petrović, I. (2011), 'Two-way D* Algorithm for Path Planning and Replanning', *Robotics and Autonomous Systems*, 59(5), 329–342.

Delius, D.M., and Burgard, W. (2010), 'Maximum-likelihood Sample-based Maps for Mobilerobots', *Robotics and Autonomous Systems*, 58(2), 133–139.

Diosi, A., and Kleeman, L. (2007), 'Fast Laser Scan Matching Using Polar Coordinates', *The International Journal of Robotics Research*, 26(10), 1125–1153.

Dissanayake, M., Newman, P., Clark, S., Durrant-Whyte, H., and Csorba, M. (2001), 'A Solution to the Simultaneous Localization and Map Building (SLAM) Problem', *IEEE Transactions on Robotics and Automation*, 17(3), 229–241.

Durrant-Whyte, H., and Bailey, T. (2006), 'Simultaneous Localization and Mapping: Part I', *IEEE Robotics & Automation Magazine*, 13(2), 99–110.

Garulli, A., Giannitrapani, A., Rossi, A., and Vicino, A. (2005), 'Mobile Robot SLAM for Line-based Environment Representation', in *44th IEEE Conference on Decision and Control, 2005 and 2005 European Control Conference. CDC-ECC '05*, pp. 2041–2046.

Giesler, B., Graf, R., Dillmann, R., and Weiman, C.F.R. (1998), 'Fast Mapping Using the Log-Hough Transformation', in *IEEE/RSJ International Conference on Intelligent Robots and Systems, 1998. Proceedings*, vol. 3, pp. 1702–1707.

Hartikainen, J., Solin, A., and Särkkä, S. (2011), *Optimal Filtering With Kalman Filters and Smoothers, a Manual for the Matlab Toolbox EKF/UKF*, Espoo: Department of Biomedical Engineering and Computational Science, Aalto University School of Science.

Julier, S.J. (1997), 'Process Models for the Navigation of High-Speed Land Vehicles', Ph.D. thesis, Robotics Research Group, University of Oxford.

Larsson, U., Forsberg, J., and Wernersson, A. (1996), 'Mobile Robot Localization: Integrating Measurements From a Time-of-flight Laser', *IEEE Transactions on Industrial Electronics*, 43(3), 422–431.

Latecki, L.J., Sobel, M., and Lakaemper, R. (2009), 'Piecewise Linear Models With Guaranteed Closeness to the Data', *IEEE Transactions Pattern Analysis and Machine Intelligence (PAMI)*, 31(8), 1525–1531.

Lee, D., and Chung, W. (2006), 'Discrete-Status-Based Localization for Indoor Service Robots', *IEEE Transactions on Industrial Electronics*, 53(5), 1737–1746.

MobileRobots, Inc. (2009), *ARNL Installation & Operations Manual*, Amherst, NH: Author.

Nguyen, V., Gächter, S., Martinelli, A., Tomatis, N., and Siegwart, R. (2007), 'A Comparison of Line Extraction Algorithms Using 2D Range Data for Indoor Mobile Robotics', *Autonomous Robots*, 23(2), 97–111.

Pfister, S.T., Roumeliotis, S.I., and Burdick, J.W. (2003), 'Weighted Line Fitting Algorithms for Mobile Robot Map Building and Efficient Data Representation', in *IEEE International Conference on Robotics and Automation, 2003. Proceedings. ICRA '03*, vol. 1, pp. 1304–1311.

Pozna, C., Troester, F., Precup, R.E., Tar, J.K., and Preitl, S. (2009), 'On the Design of an Obstacle Avoiding Trajectory: Method and Simulation', *Mathematics and Computers in Simulation*, 79(7), 2211–2226.

Rofer, T. (2002), 'Using Histogram Correlation to Create Consistent Laser Scan Maps', in *IEEE/RSJ International Conference on Intelligent Robots and System, 2002*, vol. 1, pp. 625–630.

Sakai, A., and Kuroda, Y. (2010), 'Discriminatively Trained Unscented Kalman Filter for Mobile Robot Localization', *Journal of Advanced Research in Mechanical Engineering*, 1(3), 153–161.

Schiele, B., and Crowley, J.L. (1994), 'A Comparison of Position Estimation Techniques Using Occupancy Grids', *Robotics and Autonomous Systems*, 12(3–4), 163–172.

Teslić, L., Škrjanc, I., and Klančar, G. (2010a), 'EKF-based Localisation of a Wheeled Mobile Robot in Structured Environments', *Journal of Intelligent and Robotic Systems*, 62(2), 187–203.

Teslić, L., Škrjanc, I., and Klančar, G. (2010b), 'Using a LRF Sensor in the Kalman-filtering-Based Localization of a Mobile Robot', *ISA Transactions*, 49(1), 145–153.

Thrun, S. (2002), 'Robotic Mapping: A Survey', in *Exploring Artificial Intelligence in the New Millenium*, eds. G. Lakemeyer and B. Nebel, San Francisco, CA: Morgan Kaufmann, pp. 1–36.

Tomatis, N., Nourbakhsh, I., and Siegwart, R. (2003), 'Hybrid Simultaneous Localization and Map Building: A Natural Integration of Topological and Metric', *Robotics and Autonomous Systems*, 44(1), 3–14.

Veeck, M., and Veeck, W. (2004), 'Learning Polyline Maps From Range Scan Data Acquired With Mobile Robots', in *2004 IEEE/RSJ International Conference on Intelligent Robots and Systems, 2004. (IROS 2004). Proceedings*, vol. 2, pp. 1065–1070.

Wu, H., and Qin, S.Y. (2011), 'An Approach to Robot SLAM Based on Incremental Appearance Learning With Omnidirectional Vision', *International Journal of Systems Science*, 42(3), 1617–1628.

Xu, D., Han, L., Tan, M., and Li, Y.F. (2009), 'Ceiling-Based Visual Positioning for an Indoor Mobile Robot With Monocular Vision', *IEEE Transactions on Industrial Electronics*, 56(5), 1617–1628.

Zhang, X., Rad, A.B., and Wong, Y.K. (2008), 'A Robust Regression Model for Simultaneous Localization and Mapping in Autonomous Mobile Robot', *Journal of Intelligent and Robotic Systems*, 53(2), 183–202.